Incorporation of minor constituents into Portland cement tricalcium silicate

INCORPORATION OF MINOR CONSTITUENTS INTO PORTLAND CEMENT TRICALCIUM SILICATE: BOND VALENCE ASSESSMENT OF THE ALITE M1 POLYMORPH CRYSTAL STRUCTURE USING SYNCHROTRON XRPD DATA

W. V. Fernandes[a], S.M. Torres[a]*, C.A. Kirk[b], Leal, A. F. [a], Lima Filho, M.R. [a] and Diniz, D. [a]

[a] Postgraduate Programme of Materials Science and Engineering, Federal University of Paraíba, Brazil

[b] School of Chemistry, University of Edinburgh, UK

*sandro.marden@pq.cnpq.br

ABSTRACT

Six industrial clinker samples, produced using petroleum coke as kiln fuel, were analysed using high resolution synchrotron XRPD data, one sample (HM) presenting predominantly M1 C_3S polymorph. Refinement of data collected on this sample was used to revise the M1 structural model, improving the R_{wp} and R_B of the original model (from R_{wp}=9.25 and R_B=5.517 in the original model to R_{wp}=8.07 and R_B=2.965). The revised model was validated through bond length and Bond Valence Sum (BVS) distribution. Using the BVS method, two preferential substitutional calcium sites were identified for Mg^{2+} and two silicon sites for Al^{3+}, while two interstitial sites were identified for S^{6+} and Fe^{3+}. Using the revised model for refinement of the six industrial clinker samples showed improvement in

the Rwp and GoF indices. The amount of M1 and M3 polymorph present was found to be significantly different using the revised M1 C_3S model.

Keywords: Synchrotron; Crystal structure (B); X-ray diffraction (B); Ca_3SiO_5 (D); Clinker (D).

1 INTRODUCTION

1.1 Research Background

Portland cement plants worldwide have increased the use of alternative fuels as one possible route to achieve the targeted reduction of CO_2 emissions as stated by environmental policies [1,2]. However, the use of alternative fuels (e.g. biomass, coke) might impose potential changes in the clinker composition and performance due to the incorporation of foreign elements. Petroleum coke, which is widely used as kiln fuel by cement plants in Brazil, and other alternative waste fuels, sewage sludge and bone meal for instance, mostly used in Europe, contain significant amount of sulfur [3,4].

The interaction of minor constituents must, therefore, be systematically examined. Studies report they might interact with clinker phases, altering the crystal structures and/or polymorph that is stabilized [5]. When in small amounts (<1%), these elements are

unlikely to form new phases, but may incorporate into certain clinker phases and form solid solutions. Therefore, foreign ions, originating from alternative fuels or the raw materials, can influence the distribution and nature of clinker phases formed [6]. Furthermore, studies have shown that incorporation of some metals by clinker phases have upper limits [7]. However, there are no crystal models which actually indicate whether there are preferential sites these foreign metal ions may occupy, which suggests this process can be random. Whether such incorporation might then be linked with hydration, mechanical and durability issues still demands further and systematic investigations. For instance, there is evidence to show that sulfur not only may influence the structure of clinker phases, but may also affect the mechanical properties of Portland cement, as well as play a role in alite polymorphism. Indeed, there has been indication that some polymorphs can be more reactive and, hence, some performance changes are expected [8]. Whether or not this would impose significant changes in mechanical and durability performances is also a matter or further investigation. Therefore, understanding the role minor constituents have in the stabilization of C_3S polymorphs is vital for the implementation of alternative fuels, during clinker production, as a sustainable strategy worldwide.

1.2 Minor constituents in Portland cement tri-calcium silicate

Tri-calcium silicate (Ca_3SiO_5 or C_3S) constitutes around 50% to 70% of un-hydrated Portland cement clinker by mass, being responsible for early age strength development during hydration of Portland cement based composites. There are seven known temperature dependent C_3S polymorphs in ascending temperature order: three triclinic (T1, T2, T3), three monoclinic (M1, M2, M3) and one trigonal (R) [9].

It is known that metastable phases can be stabilised for indefinite time periods through heat treatment or incorporation of chemical impurities [10]. For instance, there are studies to show that Mg tends to stabilize the M3 alite polymorph, whereas S has been shown to stabilize M1 [11–13]. The occurrence of two different polymorphic zones in the same alite crystal is not rare in ordinary Portland cements [14]. The incorporation of Mg^{2+} into the M3 alite crystal structure is through substitution of Ca^{2+}, with a suggestion of a substitution saturation level [9]. Also, as reported by Maki *et al* [15] , Fe^{3+} and Al^{3+} are shown to be linked with the incorporation of S within the structure of M1 alite. Atomistic simulations demonstrated that alite and belite crystal structures can be modified by incorporation/substitution of foreign ions, predicting that Al^{3+}, Fe^{3+} and Mg^{2+} ions could influence the calcium to oxygen bond lengths, whilst only the orientation of SiO_4^{4-} tetrahedra would be affected [16]. Consequently, changes in dissolution rate of clinker phases may be expected due to the structural changes following the incorporation of minor constituents. The orientation of the silicon tetrahedra was previously reported as noticeably different between alite polymorphs, as well as changes in coordination number of the Ca^{2+} sites, which seem to be connected to the hydration reaction [9]. Investigations

into the mechanism of solid solution formation of alite with foreign elements in industrial clinkers are required. Studies of silicon substitution by minor constituents in alite and belite phases through the use of ^{27}Al magic angle spinning (MAS) NMR have been carried out [17,18]. However, uncertainty remains within the available structural models as to whether the minor constituents in C_3S occupy sites randomly or there are preferential sites that such elements could occupy. Indeed, no published reference addressing whether any mechanism controls the incorporation was found, to the best of the authors' knowledge.

1.3 Quantitative Crystalline Phase Analysis applied to Portland cement tri-calcium silicate

Although X-ray fluorescence is the favoured technique for quality control in cement plants, Quantitative Phase Analysis (QPA) of X-ray Powder Diffraction (XRPD) data through the application of Rietveld refinement gives a more comprehensive understanding of clinker composition. Reliable crystal structure models are required in order to give enhanced comprehension of how minor constituents are present as well as to separate pure phases from solid solutions with clinker phases. However, one of the requirements of this technique is the availability of good quality structural models [19,20].

In terms of tri-calcium silicate, the selection criteria of clinker structural models is well discussed in the literature [21]. Structural determination of T3 and M3 polymorphs were possible through refinement of synchrotron XRPD data collected on synthetic clinker samples [12,22]. Synchrotron sources produce an intense and highly collimated radiation, which, when used for diffraction studies allows high quality and high resolution data to be collected. This is important when analysing industrial samples that are mostly multi-phase and have overlapping diffraction peaks [23]. Therefore, one could question the reliability of the M1 polymorph structural model, which was not determined using data collected from a high resolution radiation source [24]. In terms of assessing contamination levels of minor constituents within the crystal structure, it is important to highlight the need to understand whether any preferential substitutional sites as well as an occupation factor could assigned. To date, no published model was reported which include preferred sites for the incorporation of minor constituents, to the best knowledge of the authors [5].

1.4 Bond Valence Method applied to Portland cement tri-calcium silicate

Studying the incorporation of minor constituents into a known phase can be challenging, given the low levels of substitution or incorporation. This is especially so when the crystal structure contains many atomic positions, which could potentially allow substitution of the minor constituent, as in the case of C_3S. Another aspect to be considered is the possibility of interstitial sites, which could also allow incorporation of minor constituents.

When analysing complex structures, the use of rigid body restraints should take into account realistic bond lengths and coordination environments as well the charge of the ion on the crystallographic sites [19,20]. The Bond Valence (BV) theory offers a way of taking into account interatomic distances to estimate the bonding strength of a cation surrounded by anions using the observed bond lengths of the coordination polyhedra [25]. Therefore, it is possible to validate a new crystal structural model through the comparison of the observed bond distances with reliable crystallographic data [26,27]. Bond valence theory has been used for the validation of complex crystal structural models of inorganic oxides [28]. Furthermore, analysis of preferential substitution of crystallographic sites in a structural model, through the use of the Bond Valence Sum (BVS) method, has been previously used. For instance, in the case of Ca^{2+} substitution in apatite-group minerals, where bond valence is used to study the occupancy equilibrium of the two elements under consideration.[29,30]. To the best knowledge of the authors, the BVS method has not yet been applied to either C_3S polymorphism or the analysis of minor constituents in clinker phases.

The present work aims to use Rietveld analysis and the Bond Valence method to evaluate the C_3S M1 polymorph structure as well as to investigate potential sites for minor constituents (Mg, S, Al and Fe) to occupy within its crystal structure. Also, this paper deals with the study of minor constituents in a M1 containing industrial clinker, using the revised M1 structural model, as described here. This paper is part of a comprehensive study on the influence of minor constituents on the microstructure and reactivity of clinker phases, covering synthetic and industrial samples.

2 METHODOLOGY

Sampling: A total of 190 clinker samples were analysed in this work, which were produced by an industrial plant with a rotary kiln, 4 m in diameter and a total length of 60 m, equipped with a 5 stage cyclone tower, using petroleum coke as kiln fuel, with a 2600 ton/day production capacity and an energy consumption of 350 kW of electric power. Each sample was formed by collecting clinker pellets from the furnace output 5 times every 10 minutes, which were then mixed, resulting in a total sample weight of approximately 2 kg, and packed in a vacuum sealed plastic bag.

Six samples were selected for more detailed study, covering the composition limits of Mg and S of the industrial clinker production (Figure 1). A sample presenting the highest predominance of the C_3S M1 polymorph (HM) was chosen in order to evaluate the C_3S M1 crystal structural model.

Grinding Procedures: The clinker pellets were ground in a Herzog HSM 100P pulverizing mill equipped with a tungsten carbide grinding vessel and fully sieved through a 38 µm aperture size sieve.

Bulk chemical composition via Wave Dispersive X-ray Fluorescence (WD-XRF): Clinker samples were mixed with lithium tetraborate (67 wt%) and lithium metaborate (33 wt%) and mechanically homogenised, before being melted in a platinum crucible at 1100±10°C in a fusing machine. The molten mixture was formed into a disc using a platinum die. The fused discs were analysed by means of X-ray fluorescence (WDS-XRF) using a PANalytical™ Axios Max system.

High resolution synchrotron powder X-ray diffraction: Pulverized clinker powder samples (diameter < 38μm) were analysed on the high resolution powder diffraction beamline I11 at the Diamond Light Source synchrotron, UK [31]. The samples were packed into 0.5 mm borosilicate capillary tubes. Data were collected in transmission geometry using multi-analysing crystal (MAC) device over an angular range of 1 – 150º 2θ with a step size of 0.003° and 1200 sec total counting time using a wavelength of 82.5258 pm at room temperature and pressure. .

Revision of M1 structural model: Initially, multi-phase Rietveld refinement of the XRPD data collected on the sample with the highest predominance of C_3S M1 polymorph (HM, see figure 1) was carried out to quantify the proportions of crystalline phases present, using the software package Topas V4 [32]. The unit cell parameters of the C_2S structural model were fixed at this point in the refinement, as this phase presents strong overlapping peaks with C_3S M1 polymorph. Secondly, revision of the M1 structural model

was carried out through refinement of rigid-bodies to determine new atomic coordinates and unit cell parameters. Afterwards, the unit cell parameters of C_2S structural model were refined. The sources of the structural models used for the Rietveld refinement are shown in Table 1.

Table 1 Structural model of phases used in Rietveld refinement of clinker samples.

Phase	Formula	ICSD number	Reference
Alite/M1	Ca_3SiO_5	-	[24]
Alite/M3	Ca_3SiO_5	94742	[22]
Belite/β	Ca_2SiO_4	81096	[33]
Aluminate/cubic	$Ca_3Al_2O_6$	1841	[34]
Ferrite	Ca_2AlFeO_5	9197	[35]
Periclase	MgO	9863	[36]

Quantitative Phase Analysis from XRPD: Phase identification and quantification were carried out through Rietveld Refinement of the synchrotron XRPD data using Topas V4 software. The quality of fitting was calculated by the software using R-weighted pattern (Rwp), goodness of fit (GOF) and R-Bragg (R_B) using Equations (1), (2) and (3), as described by Coelho [37].

$$R_{wp} = (\Sigma w_m(Y_{o,m}-Y_{c,m})^2/\Sigma_{wm}Y_{o,m}^2)^{1/2} \quad (1)$$

$$GOF = \chi^2 = (\Sigma w_m(Y_{o,m}-Y_{c,m})^2/M-P)^{1/2} \quad (2)$$

$$R_B=\Sigma|I''_{o'',k}-I_{c,k}|/\Sigma I''_{o'',k} \quad (3)$$

200 $Y_{o,m}$ and $Y_{c,m}$ are the observed and calculated intensities respectively at data point m, M the number of data points, P the number of parameters, w_m the weighting given to data point m which for counting statistics is given by $w_m = s(Y_{o,m})^2$, where $s(Y_{o,m})^2$ is the error in $Y_{o,m}$. The $I_{"o",k}$ and $I_{c,k}$ are the "observed" and calculated intensities of the k_{th} reflection, respectively.

205

Bond lengths of the revised M1 structural model: Data were refined using the Noirfontaine model as a starting point [24]. The review process consisted of introducing new rigid body constraints. Detailed Rietveld refinement strategy is presented in supporting information (Table SI-1). In order to produce a modified M1 structural model, the polyhedral Ca-O and
210 Si-O bond lengths were allowed to vary according to the limits showed in Table 2 [26]. The silicon tetrahedral rotation and displacement were also refined.

Table 2 Bond length limits of calcium, silicon, magnesium and aluminium bonded to oxygen as according to the literature [26,27].

Cation	Coordination number	Minimum (pm)	Mean (pm)	Maximum (pm)
	6	221.0	237.1	284.7
Ca^{2+}	7	212.4	244.8	314.0
	8	214.9	249.8	317.6
Mg^{2+}	6	193.5	208.9	249.7
Si^{4+}	4	156.0	162.5	172.6

Al^{3+}	4	168.5	174.6	182.7

The rotation and displacement of 9 Ca_6O octahedral rigid bodies with oxygen in the center were refined. These are organized in 3 groups defined as trimers. This unusual structural description was previously reported to be present in all tricalcium silicate polymorphs [5]. Crystallographic structural diagrams, before and after refinement of rigid bodies, were produced using the software VESTA 3 [38].

Bond Valence Calculations: The Bond Valence (BV) equation (4) and respective coefficients used in this work is after Brown and Altermatt [39]:

$$s_{ij} = \exp[(R_o - R_{ij})b] \quad (4)$$

s_{ij} is bond valence between atoms i and j in valence units (v.u.), R_{ij} is the observed bond length between atoms i and j in pm, while R_0 and b, are the bond length with a unit value and the slope of the curve, respectively and have tabulated values [39]. The BVS, in valence units (v.u.), of calcium and silicon sites were obtained summing BV of each bond in the coordination polyhedra. The error regarding the difference between the expected oxidation state and BVS was also calculated.

Mean Absolute Error (MAE): The Mean Absolute Error (MAE) of BVS was used as a metric to evaluate model performance [40, 41], using equation (5). In the new proposed model, those sites with BVS above the MAE have been selected as potential substitutional sites.

MAE = $\Sigma^{n}_{i=1}|V_i-\Sigma_j s_{ij}|/n$(5), where V_i is the valence of the cation i and n is the number of cations of type i. The sum Σ_j is over all the bonds formed between atoms i and j within the i^{th} coordination polyhedra, while the sum $\Sigma^{n}_{i=1}$ is over all atoms of type i. It is normal to have some BVS deviation around the valence of an ion in a structural model. However, micro-strain or impurities may be associated with higher deviations. Therefore, MAE was tested as a statistic tool to possibly identify those crystallographic sites with the highest deviations.

Calculation of the Occupancy Factor of the Minor Constituent Ions: The equilibrium site occupancy factor of both cations was obtained via equalizing the BVS to their charges [29]. The occupation of the two ions (1 and 2) were calculated by equations (6) and (7) as reported by Brown [25]:

$p1 = (\Sigma s_2-V_2)/[(V_1-V_2)-(\Sigma s_1-\Sigma s_2)]$ (6) and

$p2 = 1-p1$ (7), where p1 and p2 are the occupancy factors and V_1 and V_2 are the atomic valences of ions 1 and 2, respectively. $\mathbb{S}s_1$ and $\mathbb{S}s_2$ are the bond valence sum (BVS) over all the bonds formed between O and atoms 1 and 2, respectively, within the

corresponding coordination polyhedra, calculated using equation (4), assuming full site occupation.

Identification of interstitial sites was performed through visual search of tetrahedral voids between pairs of silicon tetrahedra in the new model. Occupation of these interstitial sites by foreign ions was estimated using the BVS method. The foreign cations selected were Mg, Al, Fe and S, in order to account for the chemical composition of the alite phase as determined by the spot analyses using EPMA. It should be noted there are other minor constituents, present in smaller amounts, however, the above ions have been chosen due to the amount and their reported influence on M1 alite polymorph properties [15,42].Some studies have shown that P might be incorporated into the C_2S and C_3Sphases [43–45]. However, there is evidence showing that C2S silicon sites can incorporate higher amounts of P than those of C3S [18]. Therefore, incorporation of P was not considered in this study. K and Na were also not investigated as it is more probable to these ions incorporate into C_3A phase [46]. The total amount of minor constituents calculated to be present in the model, through occupancy of proposed preferential crystallographic sites as obtained through the BVS method, were compared to values obtained through spot analysis using EPMA.

Chemical Spot Analysis via EPMA: A (diamond) polished section of an industrial clinker sample has been analysed. The spot analysis was made using a Cameca SX100 instrument equipped with five vertical crystal spectrometers, a PGT Spirit energy dispersive analyser.

Amounts of constituents were determined using the Cameca PeakSight software, allowing the calculation of cation/Ca ratio of analysed crystals. This was then compared to that obtained through BVS calculation.

Effects of using Revised M1 Model for Rietveld Quantitative Phase Analysis (RQPA):

Rietveld refinement of XRPD data collected on six industrial clinker samples was initially carried out using the structural models shown in Table 2. The procedure was repeated substituting the C_3S M1 polymorph with the revised model, reported here. The same refinement strategy was adopted in both cases, following previously reported strategies [21]. Phases present in high proportions (>20 wt%), or those with narrow and little overlap in peaks, were introduced first. The refinement sequence was scale factor, background, peak shape and unit cell parameters. Subsequently, phases present in low proportions (<5%), or those with strong overlap of peaks, were added, refining sequentially the peak shape and unit cell parameters.

3 RESULTS

3.1 Chemical composition

Figure 1 shows a plot of weight percent MgO of clinker samples versus weight percent SO_3, from the composition of the petroleum coke used as kiln fuel, as determined by WD-XRF. This figure also highlights the selected six samples for detailed study, representing the Mg and S clinker compositional range of industrial production. The bulk chemical composition (weight %) of the six samples from XRF analysis is presented in Table 3. The presence of SO_3 in clinker samples is expected due to the use of petroleum coke as alternative fuel, and the SO_3 composition in relation to the coke used to produce each sample is also shown in Table 3.

[FIGURE 1]

Table 3 Bulk chemical composition of industrial clinker samples from WD-XRF.

Sample	SO_3 Coke[1]	SiO_2	Al_2O_3	Fe_2O_3	CaO	MgO	SO_3	Na_2O	K_2O	P_2O_5
ML	1.78	20.61	4.83	2.62	66.29	3.81	0.48	0.03	0.54	0.39
LM	0.59	19.94	4.76	2.63	63.62	6.98	0.55	0.01	0.72	0.39
LH	0.59	19.19	4.66	2.51	61.46	10.12	0.62	0.01	0.62	0.41
HH	2.56	19.42	4.66	2.59	61.35	9.41	1.1	0.01	0.66	0.40
HM	2.56	19.99	4.83	2.67	63.12	6.00	1.85	0.01	0.76	0.36
HL	2.35	20.99	4.84	2.72	66.23	2.78	0.97	0.02	0.69	0.38

3.2 Revision of M1 structural model

[1] This amount refers to the coke used in the kiln fuel to produce the sample.

Figure 2a shows the output from multiphase refinement of the synchrotron XRPD data of the HM sample using the Noirfontaine M1 Alite model. Whereas, Figure 2b shows the output from the refinement using the revised M1 alite model (as described below). Supporting information (Figure SI-1) shows a high angle range of XRPD data (34 to 62 2θ°), where peak overlapping is usually strong. This observed-calculated- difference plot, after Rietveld refinement, shows it is possible to clearly identify reflections even with small d-spacing (141 to 80 pm) due to high resolution of the X-ray source.

[FIGURE 2]

The phases identified were those expected for an industrial clinker sample and the multi-phase Rietveld refinement produced realistic R_{wp} values (Table 4). Although Rietveld refinement of the data led to satisfactory goodness of fit (2.17), some reflection intensities have not been well described using the Noirfontaine M1 alite model, as noticed in the difference plot in the 2 theta range 15-20° (Fig 2).

Table 4 Comparison of refinement parameters using Noirfontaine's and the revised M1 model.

Parameters	Noirfontaine's	New model
R_{wp}	9.25	8.07
GOF	2.17	1.89
R_B	5.517	2.965
Mean average error (MAE) of Ca BVS (v.u.)	0.70	0.25
Density (g/cm³)	3.15922(19)	3.15881(15)
Volume (nm³)	2.16012(13)	2.160395(99)
Mass	4109.678	4109.678
Z	9	9
a (nm)	2.783497(82)	2.783434(59)
B (nm)	0.706220(22)	0.706251(18)
C (nm)	1.223296(40)	1.223353(30)
Beta	116.0664(33)	116.0591(24)

Through the introduction and refinement of rigid bodies (Ca_6O and SiO_4 polyhedra) of the M1 polymorph, the observed-calculated fit was shown to improve, especially in terms of the fit to the most intense reflections (2 theta range 15-20 °) as well as a reduction in the number of unmatched peaks (Fig 2b). As well as the improved fit there was a noticeable improvement in terms of all the refinement fit parameters and especially the reduction of M1 R-Bragg index by almost 50% (Table 4), indicating this new strategy led to an improved fit to the observed data. Supporting information (Table SI-2) presents the new atomic coordinates, occupancy factors and atomic displacement parameters of the proposed revised M1 model.

Figure 3 presents a comparison of the crystal structures of the M1 polymorph from refinement of the XRPD data, whereby Fig 3a is drawn using the atomic positions of the Noirfontaine model and Fig 3b is the diagram from the revised model. This schematic view takes into account that Ca_6O maximum bond length is c.a. 290 pm. The most

noticeable difference is, for instance, the uninterrupted sequence of three Ca_6O trimers in the new model instead of alternate trimers, dimers and monomers as shown by Noirfontaine's model, which is an expected consequence of the imposed constraint of the Ca-O bond distance. Also, some changes in the orientation of the silicon tetrahedra are noticeable as well as the distortion of some Ca_6O octahedral vertices. Supporting information (Figure SI-1) shows the revised model with upper limits of Ca-O bond lengths of 280 and 270 pm fixed, highlighting that the Ca_6O octahedra, where the bonds are stretched beyond these limits, lie along the (1 0 0) and (3 0 0) preferential crystallographic planes.

[FIGURE 3]

3.3 Bond length distribution

The Ca-O bond length in both models have a skewed Gaussian distribution (Figure 4), which is in accordance with the Ca-O bond length distribution reported elsewhere [26]. In both models, the distribution peak maxima are close to the reported ideal value for six-fold coordinated Ca^{2+}, by O^{2-}, of 237.1 pm. Most of the bond lengths of the new model fall within the boundaries for calcium ion bonded to oxygen, as proposed by Gagné and Hawthorne [26,27]. It should be noted that some of the crystallographic sites occupied by

Ca^{2+} had Ca-O bond lengths lying below the observed lower limit (221.0 pm) [26], which was found in both models and more so in the Noirfontaine model.

[FIGURE 4]

In terms of the refined Si-O bond lengths, the distribution is approximately bimodal in the revised M1 structural model (Figure 5). The mean bond length was found to be 158.3 pm and most tetrahedra presented an average value of 152.5 pm. Noirfontaine's model has Si-O bond length values narrowly ranging between 161.6 pm and 162.1 pm, which correspond to values close to the average length of previously reported observations for Si bonded to oxygen in crystal structures [27]. Whilst the mean (158.3 pm) is inside the range previously observed for tetrahedrally coordinated silicon in crystal structures, the peak maxima (152.5 pm) is below the expected lower limit in the revised model [27]. This observation is possibly related to crystallographic strains induced due to the fast cooling rate during its synthesis, as well as distortions caused by the incorporation of foreign ions. The data suggests the incorporation of foreign ions can possibly impact the size and orientation of Si tetrahedra, which is suggested to stabilize the high temperature M1 polymorph at room temperature.

[FIGURE 5]

3.4 Bond Valence Calculations and Mean Absolute Error

Assessment on Ca^{2+} sites:

The histograms of BVS deviation with respect to the Ca valence being 2+, in terms of both structural models, are shown in Figure 6. It should be noted, two Ca sites of the Noirfontaine model, namely the Ca11 and Ca14 sites, were excluded due to their high calculated valences (5.14 and 5.69 respectively).The differences between the structural models are more evident when analysed in terms of the BVS method. There is an approximately normal distribution of BVS error of calcium sites from the proposed revised M1 model (Figure 6b), whereas the Noirfontaine model presents a more bimodal distribution of BVS error of the Ca sites (Figure 6a). After refinement of rigid-bodies, significant reduction in the mean absolute error (MAE) of BVS of the Ca sites was observed (see Table 4). This reduction of MAE from 0.7 to 0.25 reflects the improvement in the description of the crystal structure when imposing these restraints, as demonstrated by the distributions of Ca^{2+} and Si^{4+} - oxygen bond lengths and the polyhedral rotation and translation. The Ca sites of this complex structure present BVS deviations to varying degrees. This can be due to steric strain, introduced during the synthesis, or due the presence of minor constituents partially occupying these crystallographic sites.

Assessment on Si^{4+} sites:

Figure 7 shows the histogram of BVS error with respect to Si^{4+} valence of only the revised model, as the Si-O bond lengths of the Noirfontaine model vary only in the third decimal place. It was observed that some tetrahedral silicon sites presented minor distortions after refinement, allowing the study of substitution by minor constituents through BVS method on these sites to be carried out.

[FIGURE 6]

[FIGURE 7]

3.5 Foreign Ions Occupancy Factor Calculations

Those crystallographic sites with BVS error above MAE were considered as possible preferable sites for partial occupancy by minor constituents. Figure 8 shows a comparison of BVS calculations for all studied foreign ions (Mg^{2+}, Al^{3+}, Fe^{3+} and S^{+6}) on these sites using BVS method, highlighting on which site the cations may preferentially substitute to higher amounts.

Assessment on calcium sites:

Substitution of Ca^{2+} on sites Ca16 and Ca19 by Mg^{2+} gives a calculated maximum occupancy of 0.475 and 0.401, respectively. This substitution mechanism is in agreement with values reported in the literature [15]. The likelihood of Mg^{2+} being in a four-fold coordination environment and hence its presence on an interstitial site is low. Also, the Mg-O bond lengths are out with the limits observed in other structures for tetrahedral coordination of Mg^{2+}, which range between 190.9 to 197.7 pm [26].

Assessment on silicon sites:

Aluminium could substitute for silicon on the under-bonded sites Si5 and Si8, while sulfur and iron would most likely occupy the tetrahedral interstitial sites 1 and 2, respectively, according to Figure 8. The most probable valence state of sulfur would be S^{6+} due to the high oxidizing atmosphere inside the cement kiln and it has already been reported that S^{6+} would be four coordinate when bonded to oxygen [47, 48]. Therefore, it is chemically plausible for sulfur to partially occupy the tetrahedral interstitial site 1. In terms of iron, the divalent oxidation state was not considered due to very oxidizing atmosphere inside the kiln and only analysis using Fe^{3+} was carried out.

[FIGURE 8]

According to BVS, the calculated over-bonded Si1, Si3, Si7 and Si9 sites could be occupied by S^{6+}, if sufficient amounts of sulfur were present. However, if S were present in such quantities, the formation of separate alkali sulfate phases would be observed. On the other hand, some under-bonded sites might possibly present vacancies, reducing the occupancy factor in order to maintain charge neutrality. For instance, the formal substitution for the incorporation of aluminium and iron would be $2Al^{3+}$ or $2Fe^{3+}$ for $1Ca^{2+}$ and $1Si^{4+}$ to retain charge balance [9]. Accordingly, the incorporation mechanism of S^{6+} might be linked to the reduction of the under-bonded Mg^{2+} occupancy factor, to allow charge neutrality to be maintained. This would agree with the correlation these two ions have with alite polymorphism [9]. Equation 8 shows a chemical formula with the substitution scheme to achieve charge balance, where a, b, c and d are the sum of the occupancy factors of preferential sites for Mg^{2+}, S^{6+}, Al^{3+} and Fe^{3+}, respectively, divided by Z/2 (Z is the number of formula units and 2 is the number of symmetric site positions), while Equation 9 shows the resultant chemical formula after substitution of site occupancies. The brackets in the equations 8 and 9 mean vacancies.

$$(Ca_{3-(a+(c+d)/2)}[\ ]_a Mg_{a-3b}S_b)O_3(Si_{1-(c+d)/2}[\ ]_{(c+d)/2}Al_cFe_d)O_2 \quad (8)$$

$$(Ca_{2.769}[\ ]_{0.097}Mg_{0.043}S_{0.018})O_3(Si_{0.867}[\ ]_{0.133}Al_{0.180}Fe_{0.087})O_2 \quad (9)$$

Supporting information (Figure SI-2) shows structural diagrams of the revised model, highlighting possible preferential sites for substitution as determined by the BVS calculations. The proximity of the preferential Mg^{2+}, S^{6+}, Fe^{3+} and Al^{3+} sites possibly means that there can be clustering of foreign cations within the structure. It can also be seen that the interstitial tetrahedral sites share their vertices with two adjacent silicon tetrahedra. The atomic coordinates of the interstitial sites 1 and 2, occupied by sulfur and iron, respectively, are displayed in supporting information (Table SI-3).

3.6 Chemical spot analysis via EPMA

Using optical microscopy it was possible to identify alite crystals, as they have a known angular hexagonal morphology [9]. These crystals were then studied using SEM. A backscattered electron image of polished sections of the clinker sample HM is shown in supporting information (Figure SI-3). The points selected for spot analysis were centred on the alite crystals, to guarantee EPMA precision. Whilst darker clusters were identified as periclase (MgO), the composition of the lighter grey phase matched with the composition of ferrite (C_4AF). It was not possible to detect the presence of tricalcium aluminate (C3A), despite identification of this phase using QPA by Rietveld refinement. However, it was reported that the cubic aluminate polymorph presents smalls crystals embedded in the ferrite phase [9].

Figure 9 shows a plot of cation/Ca ratio as a function of Si/Ca ratio from data collected by EPMA. The Mg/Ca and S/Ca ratios are not significantly influenced by Si/Ca ratio, while Al/Ca and Fe/Ca show a decreasing trend as a function of Si/Ca ratio. Accordingly, incorporation of hexavalent sulfur ions should generate vacancies in order to maintain charge neutrality and this can be achieved through reduction in the occupancy of under-bonded Mg^{2+} on the over-bonded calcium sites, therefore creating vacancies. However, it is expected that increasing amounts of sulfur could be accommodated through substitution of Si^{4+} on over-bonded sites, with limitations due to the amount of vacant sites necessary to achieve charge neutrality. In order to allow vacancies, it would be reasonable to expect that increasing the sulfur content could also influence a reduction in the occupancies of under-bonded Ca^{2+} or Mg^{2+} sites.

[FIGURE 9]

The cation/Ca ratio was calculated using the occupancy factors obtained through BVS calculations and plotted along with results from EPMA (Figure 9). There are discrepancies between the results from EMPA and XRPD. XRPD is a bulk technique, which analyses average compositions throughout the sample, whereas EPMA is targeting one crystal in a sample. It is likely that there will be variability in the composition of alite crystals in the

sample and even a variation of composition within one crystal due to the growth mechanism. This is caused by changes in composition of the liquid phase inside the kiln, during the manufacturing process, as well as fast cooling rates that could hinder proper diffusion of minor constituents.

Magnesium and sulfur BVS results approximate to those from EPMA. Al and Fe show the largest differences in results from these two techniques. However, the data fit a linear trend.

3.7 *Effects of using Revised M1 model for Rietveld Quantitative Phase Analysis (RQPA)*

For all six samples, Rietveld refinement difference curves showed an improved fit to the raw data when the revised model is used. This is particularly noticeable over the 17 to 18.5 2θ range, where the strongest reflections of C_3S are observed, as shown in Figure 10. Accordingly, a notable reduction of fit indexes (Rwp and Gof) for all samples when the revised M1 model is adopted can be observed in supporting information (Figure SI-4). In most cases, the amount of M1 alite phase is higher when the revised model is used (figure 11). The exception is HM sample, presenting zero M3 content when using Noirfontaine's model. It is important to highlight that the revised model allowed identification of both M3 and M1 alite polymorphs in each sample. The total amount of alite did not showed significant differences when the revised M1 model is used; this was also the case for the

proportions of the other phases (Figure 12). It is worth to mention that C_2S beta phase amount is slightly higher when revised model is used, which might be explained by the improved resolution of revised model compared to Noirfontaine's.

[Figure 10]

[Figure 11]

[Figure 12]

4 DISCUSSIONS

The sample HM was targeted for an in-depth structural analysis of the M1 polymorph, as it contained M1 polymorph as major phase. The BVS assessment on the M1 tricalcium silicate polymorph demonstrated improvement of the existing M1 model by Noirfontaine. The instrument influence in peak shape was minimized by using high resolution synchrotron radiation obtained with multi-analysing crystal (MAC) device. However, there are still some differences in the most intense reflections when using revised M1 model. This can be explained by sample contribution for peak shape (for instance crystallite sizes, defects and micro-strain), which may vary according to diffraction angle, may not be fully described through the peak shape function [20].

The proposed model helps to assess and understand interactions of clinker phases with the minor constituents at an industrial scale, allowing a more realistic representation of an industrial M1 alite crystal structure model. The new approach allowed the proposed

model to help with the estimation of minor constituent interactions within the crystal structure. The main observations that can be drawn are detailed below.

4.1 Polyhedral bond length distribution of Alite M1 polymorph

The reliability of the new proposed model is demonstrated by the fact that all calculated bond lengths fall within reported values of related structural models [26,27], enhancing the quality of fitting. The imposed degrees of freedom implemented during refinement of the high resolution XRPD data, i.e. Si-O and Ca-O bond lengths as well as polyhedral orientation, showed significant improvement in the quality of fitting, particularly in terms of the fit indexes (R Bragg) compared to the Noirfontaine M1 model. Despite some Ca-O and Si-O bond lengths outside the reported limits, in terms of calcium silicate minerals, the range of Ca-O and Si-O interatomic distances of the new M1 model indicated that only a few sites could be available for substitutional incorporation of foreign elements. The presence of some ions cause distortions that can be linked to steric strain [25]. It should be highlighted that the fast cooling rate and burning history produce distortions within the crystal structure, stabilizing higher temperature metastable polymorphs, such as M1, at room temperature [14]. The Ca_6O octahedral motifs can give a better depiction of the presence of minor constituents, which is in agreement with previous atomistic simulations [16]. The modified model presented an uninterrupted sequence of three Ca_6O trimers along the *a*-axis of the M1 cell instead of alternating trimers, dimers and monomers as

shown by Noirfontaine's model. This can be validated by a more uniform bond length distribution as observed in other crystalline structures [26,27]. Noirfontaine's model presents some Ca-O bond lengths outside the reported range observed for six coordinate Ca^{2+} ions in minerals [26], while, in the new model, the distribution falls more within the reported range. The lower limit of Ca-O bond lengths (191.3 pm) in this revised model is likely to indicate preferable sites for incorporation/substitution of magnesium. Therefore, shorter Ca-O bond lengths resulted from the refinement as it was restricted during rigid body refinement. Hence, the Ca_6O octahedra with bond lengths outside the ideal Ca-O bond length range were allowed to adjust their linkages with the silicon tetrahedra.

4.2 BV assessment of M1 polymorph

Using BV theory to scrutinise both structural models showed the new model could help in the prediction of possible crystallographic sites, for substitution by minor constituent ions (with acceptable valences, for the studied minor constituent candidates). The prediction of minor constituent occupancy factors using BVS through Rietveld refinement provides a better description of the M1 polymorph. This approach gives support to the study of minor constituents within the crystal structure of other clinker phases. There is evidence to support the idea that the interaction of minor constituents with the C_3S M1 polymorph is limited to a few specific crystallographic sites within the crystal structure, and not random as previously indicated with other models [16].

4.3 Consequences of BV Distribution of M1 crystallographic sites for interactions of minor constituents

The variations of Si-O interatomic distances refined alongside the orientation of the tetrahedra, allowed important features of the alite crystal structure to be studied. Indeed high temperature stabilization of M1 is likely to be affected by the presence of foreign ions as well as the cooling history. The average Si-O bond length distribution was found to be bimodal, with most Si sites having a bond length to O around 156 pm, a lower limit as reported elsewhere [27]. However, the deviation in BVS distribution indicates most Si crystallographic sites are stable in terms of their valence, suggesting only a few sites may undergo limited substitution with some foreign cations, for instance aluminium.

4.4 Effects of new model in RQPA

Use of the revised model led to an improvement in the refinement of the data, evident by the reduction in the fit indexes in comparison to the refinements using the Norfontaine M1 model. Different amounts of M3 and M1 polymorph were observed when using the revised M1 model, despite only negligible differences in the total amount of C_3S and other clinker phases present. Therefore, this shows the use of the new, revised model allowed a

more reliable assessment of proportions of clinker phases present using phase quantification through Rietveld refinement of XRPD data.

The use of high flux synchrotron powder X-ray diffraction over conventional lab XRD, as used by Noirfontaine, allows much higher resolution data to be obtained due to the collimated X-ray beam and the multi-analysing crystal (MAC) device. There is an improvement in the signal:noise ratio as well as the sharpening of peaks. In a complex multi-phase system, as studied here, the high quality data allows multiphase refinements and there is greater confidence in deconvolution of overlapping peaks. In order to further demonstrate the accuracy of the refinement in resolving peak overlap in studied system, the inclusion of a revised M1 structural model allowed the identification of small amounts of M3 polymorph present in the reported sample. Both C_3S polymorph are usually present in industrial clinkers, but this observation was not possible when using Noirfontaine´s model, showing the revised model provided an adequately identification of these phases (M1 and M3).

5 CONCLUSIONS

The BVS assessment of the M1 tricalcium silicate polymorph allowed the improvement of the existing M1 model, as proposed by Noirfontaine and the main conclusions can be drawn as follows:

- By allowing the polyhedral Ca-O and Si-O bond lengths to vary according to the limits shown in Table 2 [26], as well as refining the silicon tetrahedral rotation and displacement, the revised model was able to improve the quality of fit to high resolution synchrotron X-ray powder diffraction data collected on an industrial clinker sample containing M1. The revised structural model is more feasible in that it includes Ca_6O trimers, compared to random Ca_6O monomer, dimer and trimer units in the Noirfontaine model (Fig 3).
- The revised model accounts for limited uptake of foreign elements into the studied tricalcium silicate M1 polymorph. As such, only a few crystallographic sites present bond length deviations outside the average values as reported in the recent studies on cation to oxygen bond length distributions in solid state crystalline materials and minerals [26,27]. Hence, any crystallographic sites showing such deviations may allow the co-occupancy with foreign elements. This then yields improved BVS deviations of those specific crystallographic sites.
- The revised model indicates that the interaction of minor constituents with the M1 crystal structure appears to be selective rather than random. The calculated saturation levels of each studied element, predicted by BVS calculations, do not closely correspond with the data collected using EPMA technique. This deviation may be due to this technique being less representative of a bulk sample when compared to a bulk technique such as X-ray diffraction. Therefore, despite some minor constituents may possibly be found randomly distributed when closer to crystal defects or grain boundaries, it seems likely that Mg^{2+} would substitute for

Ca^{2+}, and Al^{3+} is more likely to substitute for Si^{4+} on some sites. However, S^{6+} could theoretically substitute for Si^{4+} on some sites, but due to the requirement of charge neutrality of the compound, limitations would be imposed on the saturation levels, as it would lead to the creation of more vacant sites in order to keep charge neutrality (Fig 9). There also seems to be a possibility of Fe^{3+} and S^{6+} incorporation within some interstitial sites, again up to limited saturation levels;

- Using BVS theory, two preferential substitutional calcium sites were identified for Mg^{2+}, with maximum occupancy factors of 0.475 and 0.401, and two silicon sites for Al^{3+}, with maximum occupancy factor of 0.812 for both. Two different preferential interstitial sites were identified for S^{6+} and Fe^{3+}, with maximum occupancy factors of 0.162 and 0.782, respectively.

Overall, the revised model is much improved due to its better depiction of M1 crystal structure, highlighting preferable sites cations can occupy as well as helping to assess the influence minor constituents have on the M1 C_3S polymorph.

This paper proposes using BVS theory to validate a new approach to describe the M1 tricalcium silicate polymorph model in terms of the incorporation of foreign cations within the crystal structure, through either substitution or occupancy of interstitial sites. It can be concluded that such interactions are not random but governed by the valence equilibrium of each crystallographic site. Although the incorporation can be mostly substitutional, the occupation factor limits will depend upon the type of foreign cation on each crystallographic site. This may provide scientific basis for the investigation of the impact

the use of alternative fuels within cement kilns have on alite polymorphism. This highlights how vital crystallographic studies are to assess the role minor constituents play in cement clinker quality and performance. The interaction of most common minor constituents with other structural models of alite polymorphs using BVS method needs to be addressed, which is the subject of future work, providing an indirect method to determine the amount of multiple minor constituents inside alite phases.

6 ACKNOWLEDGEMENTS

Funding: The authors would like to thank STFC for funding the Diamond Light Source beamtime (EE17716), to Prof Chiu Tang, Dr Sarah Day and Dr Claire Murray, beamline scientists on the I11 beamline at The Diamond Light Source, for their assistance in setting up the beamline to carry out these experiments, Dr Chris Hayward for his assistance in setting up the electron probe microanalysis microscope and with the interpretation of the results, Dr. Rodinei Medeiros Gomes for his valuable comments. This work was supported by CNPq – Conselho Nacional de Desenvolvimento Científico e Tecnológico [313193/2014-2]; CAPES Foundation [PDSE - 88881.133356/2016-01; PRINT – 88887.467348/2019-00]. The authors would like to acknowledge the important contributions of CHESF-Companhia de Eletrificação do Vale do São Francisco [CTNI 92.2013.2700.00] and The Elizabeth Group - Division of Cimentos Ltda for supplying the sample and technical support.

685 6 REFERENCES

[1] L. Barcelo, J. Kline, G. Walenta, E. Gartner, Cement and carbon emissions, Mater. Struct. 47 (2014) 1055–1065. doi:10.1617/s11527-013-0114-5.

[2] E. Gartner, H. Hirao, A review of alternative approaches to the reduction of CO2
690 emissions associated with the manufacture of the binder phase in concrete, Cem. Concr. Res. 78 (2015) 126–142. doi:10.1016/j.cemconres.2015.04.012.

[3] K.L. Scrivener, V.M. John, E.M. Gartner, Eco-efficient cements: Potential economically viable solutions for a low-CO2cement-based materials industry, Cem. Concr. Res. (2018). doi:10.1016/j.cemconres.2018.03.015.

695 [4] S. Supino, O. Malandrino, M. Testa, D. Sica, Sustainability in the EU cement industry : the Italian and German experiences, J. Clean. Prod. 112 (2016) 430–442. doi:10.1016/j.jclepro.2015.09.022.

[5] H.M. Ludwig, W. Zhang, Research review of cement clinker chemistry, Cem. Concr. Res. 78 (2015) 24–37. doi:10.1016/j.cemconres.2015.05.018.

700 [6] A.K. Chatterjee, Chemistry and engineering of the clinkerization process - Incremental advances and lack of breakthroughs, Cem. Concr. Res. 41 (2011) 624–641. doi:10.1016/j.cemconres.2011.03.020.

[7] N. Gineys, G. Aouad, F. Sorrentino, D. Damidot, Threshold Limits for Trace Elements in Portland Cement Clinker, Methods. (n.d.) 2–8.

[8] H. Zhou, X. Gu, J. Sun, Z. Yu, H. Huang, Q. Wang, X. Shen, Research on the formation of M1-type alite doped with MgO and SO3—A route to improve the quality of cement clinker with a high content of MgO, Constr. Build. Mater. 182 (2018) 156–166. doi:10.1016/j.conbuildmat.2018.06.078.

[9] H.F.W. Taylor, Cement chemistry, Acad. Press. 20 (1990) 335. doi:10.1016/S0958-9465(98)00023-7.

[10] W. Callister, D. Rethwisch, Materials science and engineering: an introduction, 2010. doi:10.1016/0025-5416(87)90343-0.

[11] I. Maki, K. Kato, Phase Identification of Alite in Portland Cement Clinker, Cem. Concr. Res. 12 (1982) 93–100. doi:10.1016/0008-8846(82)90103-X.

[12] Á.G. De la Torre, R.N. De Vera, A.J.M. Cuberos, M.A.G. Aranda, Crystal structure of low magnesium-content alite: Application to Rietveld quantitative phase analysis, Cem. Concr. Res. 38 (2008) 1261–1269. doi:10.1016/j.cemconres.2008.06.005.

[13] X. Li, W. Xu, S. Wang, M. Tang, X. Shen, Effect of SO3 and MgO on Portland cement clinker: Formation of clinker phases and alite polymorphism, Constr. Build. Mater. 58 (2014) 182–192. doi:10.1016/j.conbuildmat.2014.02.029.

[14] D.E. Macphee, E.E. Lachowski, Cement Components and Their Phase Relations, in: Lea's Chem. Cem. Concr., 2003: pp. 95–129. doi:10.1016/B978-075066256-7/50015-1.

[15] I. Maki, K. Fukuda, H. Yoshida, J. Kumaki, Effect of MgO and SO3 on the Impurity

Concentration in Alite in Portland Cement Clinker, J. Am. Ceram. Soc. 75 (1992) 3163–3165. doi:10.1111/j.1151-2916.1992.tb04407.x.

[16] H. Manzano, E. Durgun, M.J. Abdolhosseine Qomi, F.J. Ulm, R.J.M. Pellenq, J.C. Grossman, Impact of chemical impurities on the crystalline cement clinker phases determined by atomistic simulations, Cryst. Growth Des. 11 (2011) 2964–2972. doi:10.1021/cg200212c.

[17] J. Skibsted, H.J. Jakobsen, C. Hall, Direct Observation of Aluminium Guest Ions in the Silicate Phases of Cement Minerals by 27AI MAS NMR Spectroscopy, J. Chem. Soc. Faraday Trans. 90 (1994) 2095–2098.

[18] S.L. Poulsen, H.J. Jakobsen, J. Skibsted, Incorporation of phosphorus guest ions in the calcium silicate phases of portland cement from 31P MAS NMR spectroscopy, Inorg. Chem. 49 (2010) 5522–5529. doi:10.1021/ic100140j.

[19] R. Young, The Rietveld Method, Int. Union Crystallogr. Oxford Sci. Publ. (1993) 312. doi:10.1017/CBO9781107415324.004.

[20] L.B. McCusker, R.B. Von Dreele, D.E. Cox, D. Louër, P. Scardi, Rietveld refinement guidelines, J. Appl. Crystallogr. 32 (1999) 36–50. doi:10.1107/S0021889898009856.

[21] Á.G. De la Torre, I. Santacruz, L. León-Reina, A. Cuesta, M.A.G. Aranda, 1. Diffraction and crystallography applied to anhydrous cements, in: H. Pöllmann (Ed.), Cem. Mater., De Gruyter, Berlin, Boston, 2017: pp. 3–29. doi:10.1515/9783110473728-002.

[22] Á.G. De La Torre, S. Bruque, J. Campo, M.A.G. Aranda, The superstructure of C3S from synchrotron and neutron powder diffraction and its role in quantitative phase analyses, Cem. Concr. Res. 32 (2002) 1347–1356. doi:10.1016/S0008-8846(02)00796-2.

[23] A.G. De la Torre, A. Cabeza, A. Calvente, S. Bruque, M.A.G. Aranda, Full phase analysis of portland clinker by penetrating synchrotron powder diffraction, Anal. Chem. 73 (2001) 151–156. doi:10.1021/ac0006674.

[24] M.N. De Noirfontaine, M. Courtial, M. De Noirfontaine, F. Dunstetter, G. Gasecki, M. Signes-Frehel, Tricalcium silicate Ca3SiO5 superstructure analysis: a route towards the structure of the M1 polymorph, Zeitschrift Für Krist. 227 (2012) 102–112. doi:10.1524/zkri.2011.1425.

[25] I.D. Brown, The Chemical Bond in Inorganic Chemistry: The Bond Valence Model, 2010. doi:10.1093/acprof:oso/9780199298815.001.0001.

[26] O.C. Gagné, F.C. Hawthorne, Bond-length distributions for ions bonded to oxygen: Alkali and alkaline-earth metals, Acta Crystallogr. Sect. B Struct. Sci. Cryst. Eng. Mater. 72 (2016) 602–625. doi:10.1107/S2052520616008507.

[27] O.C. Gagné, F.C. Hawthorne, Bond-length distributions for ions bonded to oxygen: metalloids and post-transition metals, Acta Crystallogr. Sect. B Struct. Sci. Cryst. Eng. Mater. 74 (2018) 63–68. doi:https://doi.org/10.1107/S2052520617017437.

[28] I.R. Evans, Validation of a Complex Inorganic Crystal Structure using Bond Valence

765 Restraints, Com. Crystallogr. Teach. (2007).

[29] M.E. Fleet, Y. Pan, Site preference of rare earth elements in fluorapatite, Am. Mineral. 80 (1995) 329–335. doi:10.2138/am-1995-3-414.

[30] Y. Pan, M.E. Fleet, Compositions of the Apatite-Group Minerals: Substitution Mechanisms and Controlling Factors, Rev. Mineral. Geochemistry. 48 (2002) 13–49.
770 doi:10.2138/rmg.2002.48.2.

[31] S.P. Thompson, J.E. Parker, J. Potter, T.P. Hill, A. Birt, T.M. Cobb, F. Yuan, C.C. Tang, Beamline I11 at Diamond: A new instrument for high resolution powder diffraction, Rev. Sci. Instrum. 80 (2009). doi:10.1063/1.3167217.

[32] A. Coelho, Topas 4.2, Bruker AXS GmbH. (2009).

775 [33] E.. Mumme, W.G.; Hill, R.J.; Bushnell, G.W.; Segnit, Rietveld crystal structure refinements, crystal chemistry and calculated powder diffraction data for the polymorphs of dicalcium silicate and related phases, Neues Jahrb. Fuer Mineral. Abhandlungen. 169 (1995) 35–68.

[34] J.. Mondal, P.; Jeffery, The crystal structure of tricalcium aluminate, Ca3 Al2 O6,
780 Acta Crystallogr. Sect. B Struct. Crystallogr. Cryst. Chem. 31 (1975) 689–697.

[35] S. Colville, A.A.; Geller, The crystal structure of brownmillerite, Ca2 Fe Al O5, Acta Crystallogr. Sect. B Struct. Crystallogr. Cryst. Chem. 27 (1971) 2311–2315.

[36] Y. Sasaki, S.; Fujino, K.; Takeuchi, X-ray determination of electron-density

distributions in oxides, Mg O, Mn O, Co O, and Ni O, and atomic scattering factors of their constituent atoms, Proc. Jpn. Acad. 55 (1979) 43–48.

[37] A.A. Coelho, TOPAS-Academic, Version 6: Technical Reference, (2016) 208. http://www.bruker-axs.de/.

[38] K. Momma, F. Izumi, VESTA 3 for three-dimensional visualization of crystal, volumetric and morphology data, J. Appl. Crystallogr. 44 (2011) 1272–1276. doi:10.1107/S0021889811038970.

[39] I.D. Brown, D. Altermatt, Bond-valence parameters obtained from a systematic analysis of the Inorganic Crystal Structure Database, Acta Crystallogr. Sect. B. (1985). doi:10.1107/S0108768185002063.

[40] C.J. Willmott, K. Matsuura, Advantages of the mean absolute error (MAE) over the root mean square error (RMSE) in assessing average model performance, Clim. Res. 30 (2005) 79–82. doi:10.3354/cr030079.

[41] C. Sammut, G.I. Webb, eds., Mean Absolute Error, in: Encycl. Mach. Learn., Springer US, Boston, MA, 2010: p. 652. doi:10.1007/978-0-387-30164-8_525.

[42] I. Maki, K. Fukuda, S. Seki, T. Tanioka, Impurity Distribution During Crystal Growth of Alite in Portland Cement Clinker, J. Am. Ceram. Soc. 74 (1991) 2082–2085. doi:10.1111/j.1151-2916.1991.tb08263.x.

[43] M.N. De Noirfontaine, S. Tusseau-nenez, M. Signes-frehel, G. Gasecki, C. Girod-labianca, Effect of Phosphorus Impurity on Tricalcium Silicate T 1 : From Synthesis

to Structural Characterization, J. Am. Ceram. Soc. 2344 (2009) 1–8.
805 doi:10.1111/j.1551-2916.2009.03092.x.

[44] T. Staněk, P. Sulovský, The influence of phosphorous pentoxide on the phase composition and formation of Portland clinker, Mater. Charact. 60 (2009) 749–755. doi:10.1016/j.matchar.2008.11.013.

[45] S. Boughanmi, I. Labidi, A. Megriche, M. El Maaoui, A. Nonat, Natural fluorapatite as
810 a raw material for Portland clinker, Cem. Concr. Res. 105 (2018) 72–80. doi:10.1016/j.cemconres.2018.01.006.

[46] L. Gobbo, L. Sant'Agostino, L. Garcez, C3A polymorphs related to industrial clinker alkalies content, Cem. Concr. Res. 34 (2004) 657–664. doi:10.1016/j.cemconres.2003.10.020.

815 [47] F.C. Hawthorne, S. V. Krivovichev, P.C. Burns, The Crystal Chemistry of Sulfate Minerals, Rev. Mineral. Geochemistry. 40 (2000) 1–112. doi:10.2138/rmg.2000.40.1.

[48] O.C. Gagné, F.C. Hawthorne, Bond-length distributions for ions bonded to oxygen: Results for the non-metals and discussion of lone-pair stereoactivity and the
820 polymerization of PO4: Results, Acta Crystallogr. Sect. B Struct. Sci. Cryst. Eng. Mater. 74 (2018) 79–96. doi:10.1107/S2052520617017541.

Figure 1 Plot of MgO composition of 190 clinker samples versus SO_3 composition of respective petroleum coke used as kiln fuel, from WD-XRF, highlighting the selected 6 samples for detailed study.

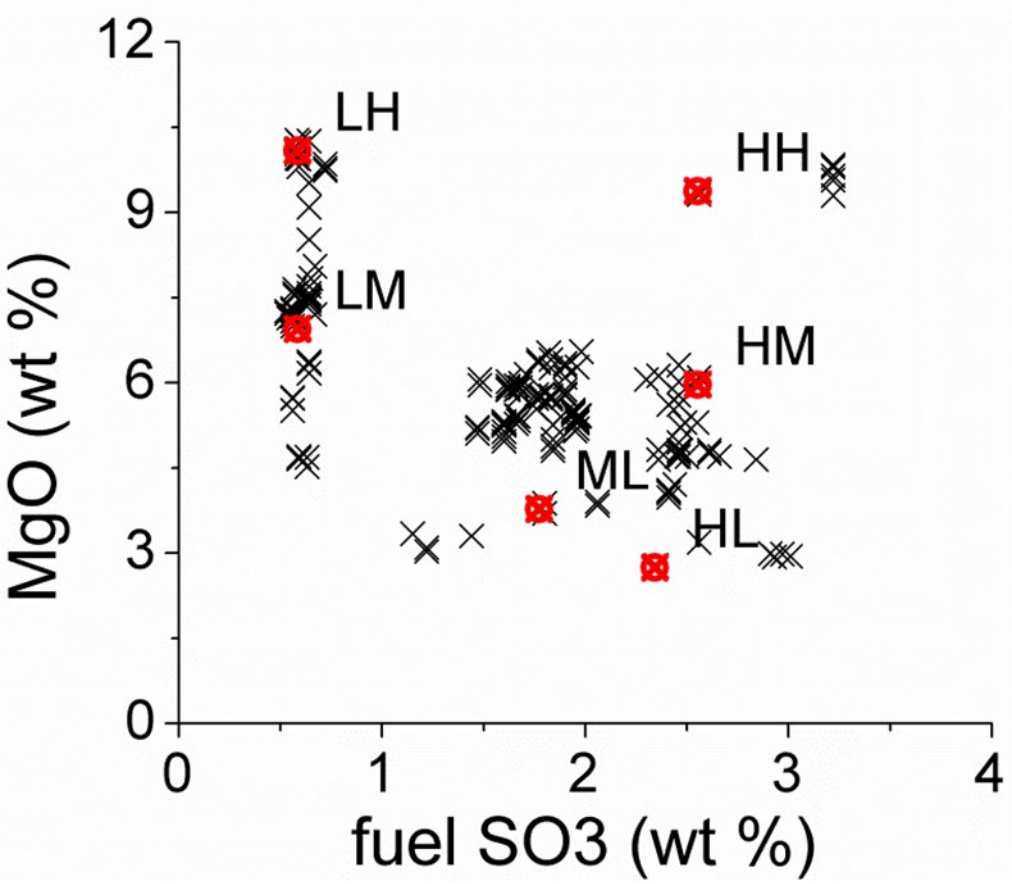

Figure 2 Comparison of the observed, calculated and difference profiles from Rietveld refinement of synchrotron PXRD data of the industrial clinker sample before (a) and after determination of revised atomic parameters for Noirfontaine's M1 Model through refinement of rigid-bodies (b).

a)

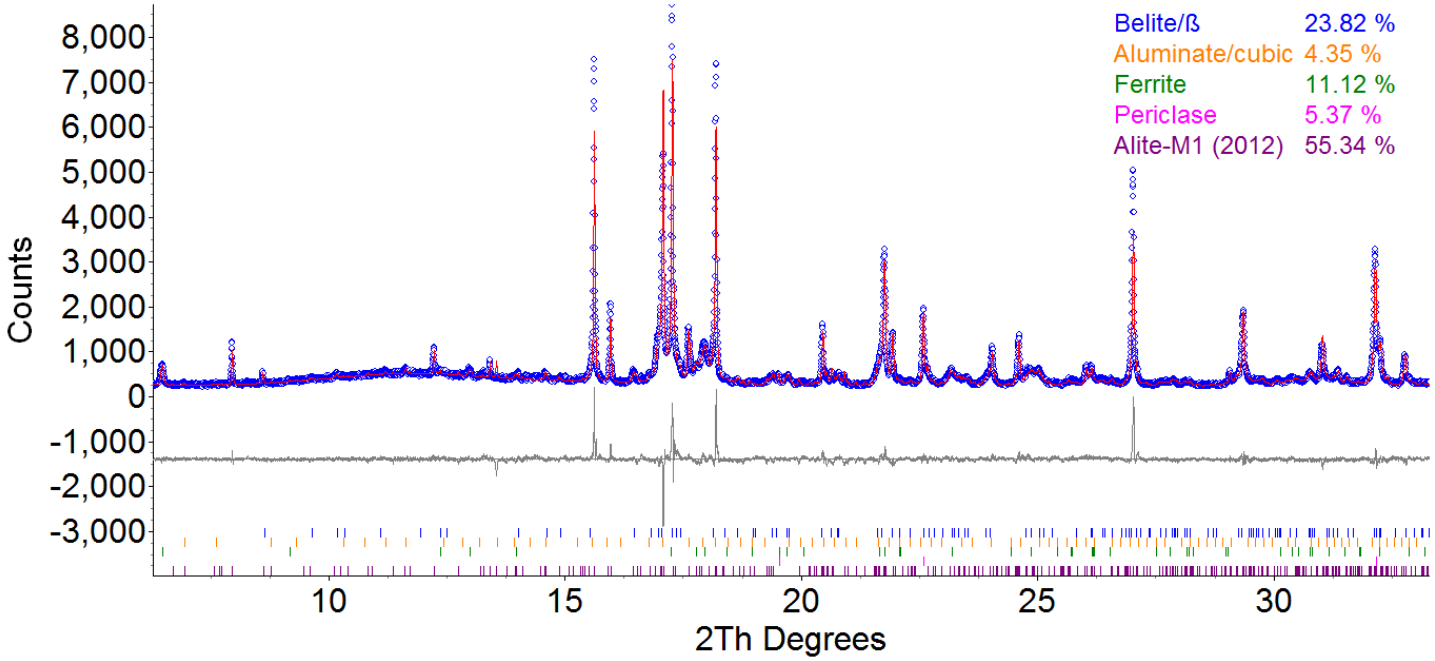

b)

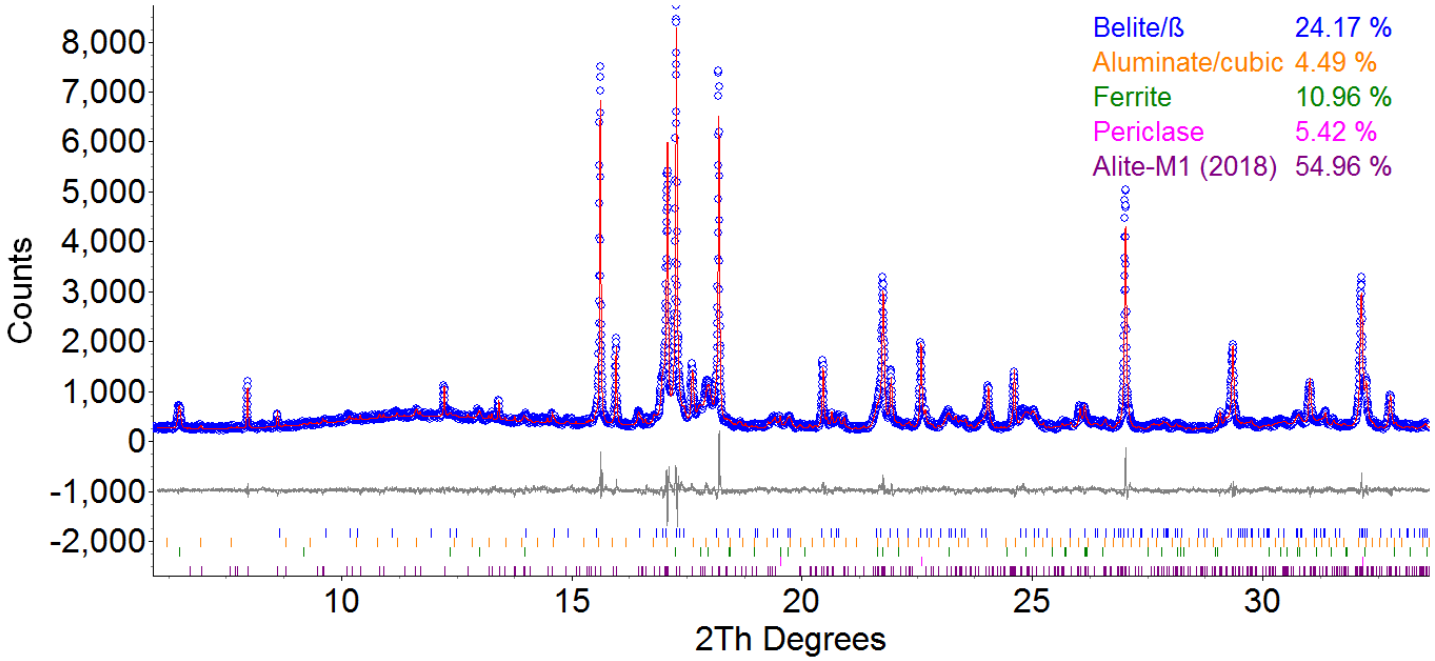

Figure 3 Crystallographic structural diagrams showing the *ac* and *bc* planes of the Noirfontaine structural model (a) compared to the new revised M1 structural model (b). Silicon surrounded by 4 oxygen atoms is represented as blue tetrahedra, while oxygen surrounded by 6 calcium atoms is represented as red octahedra.

a)

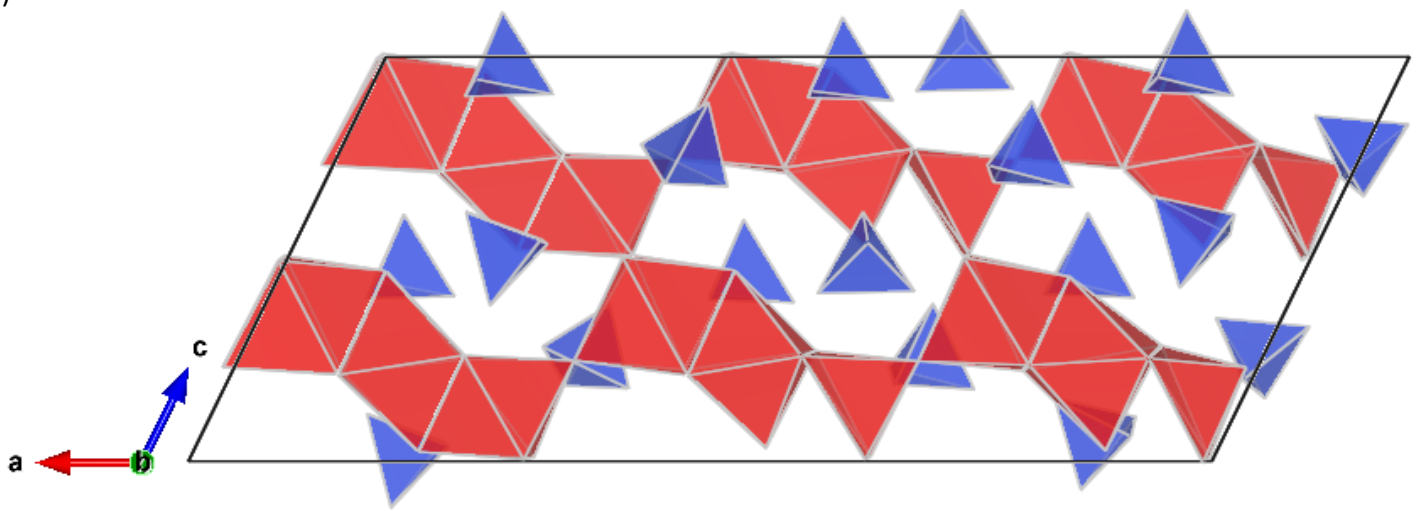

b)

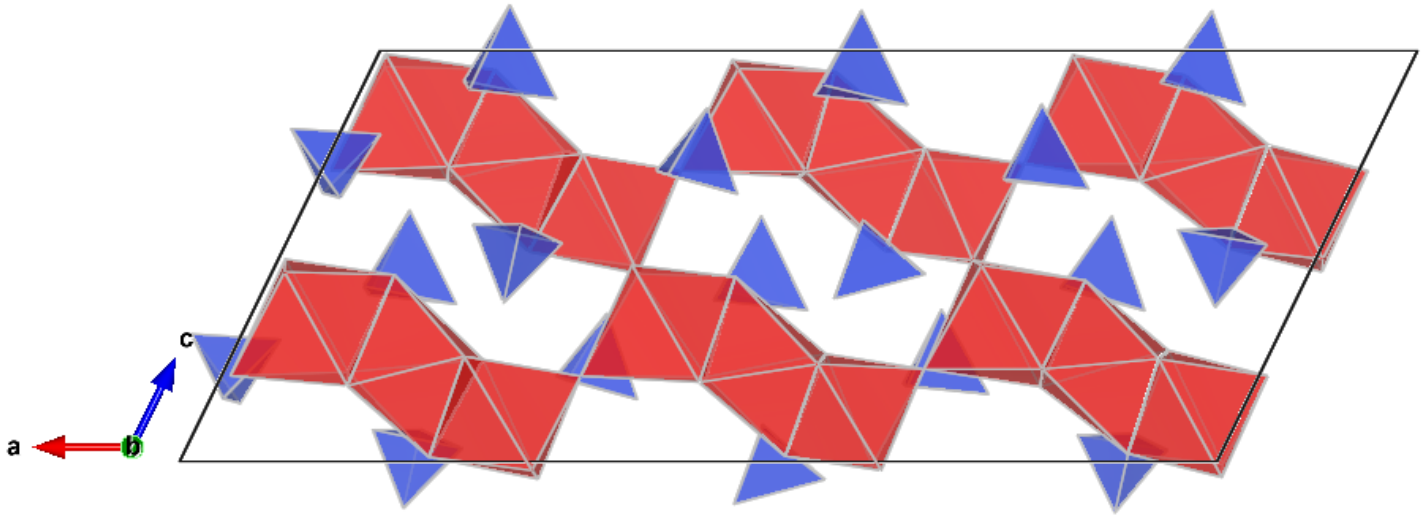

Figure 4 Distribution of Ca-O bond lengths of Noirfontaine's (a) and new proposed M1 structural model (b).

a)

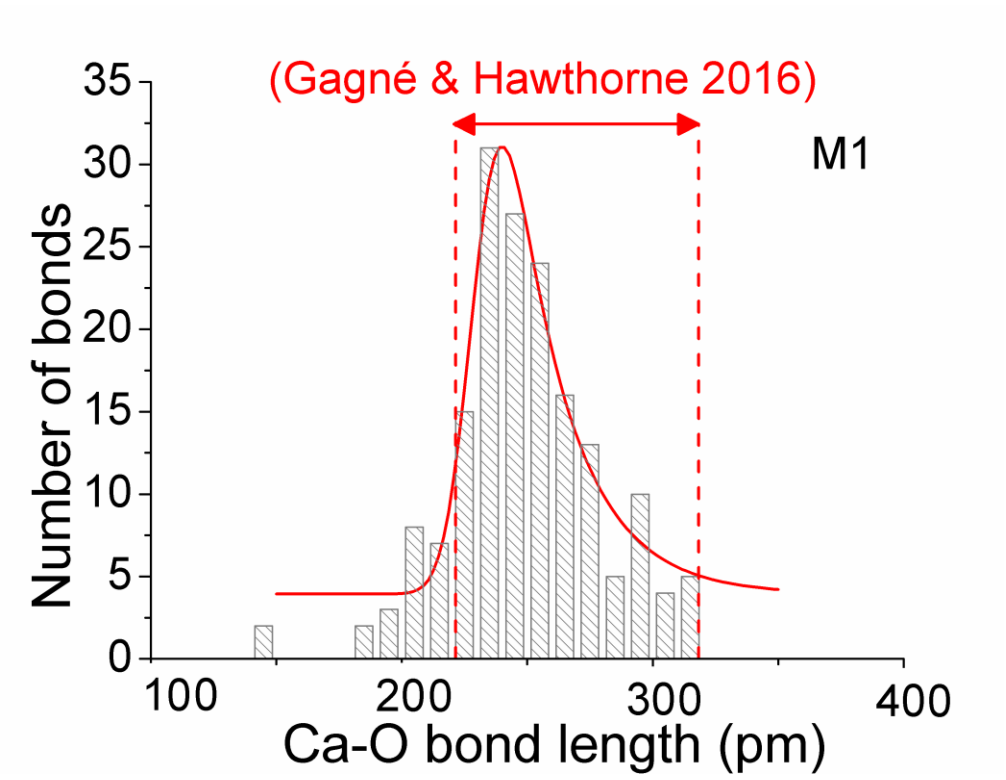

b)

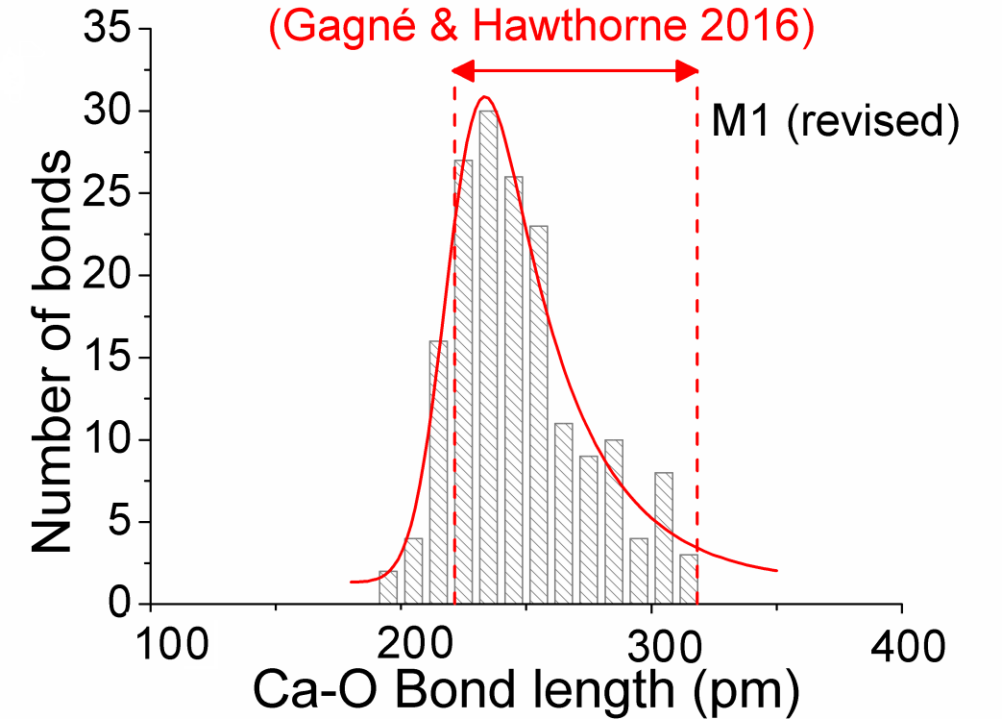

Figure 5 Distribution of Si-O bond length in new proposed M1 structural model.

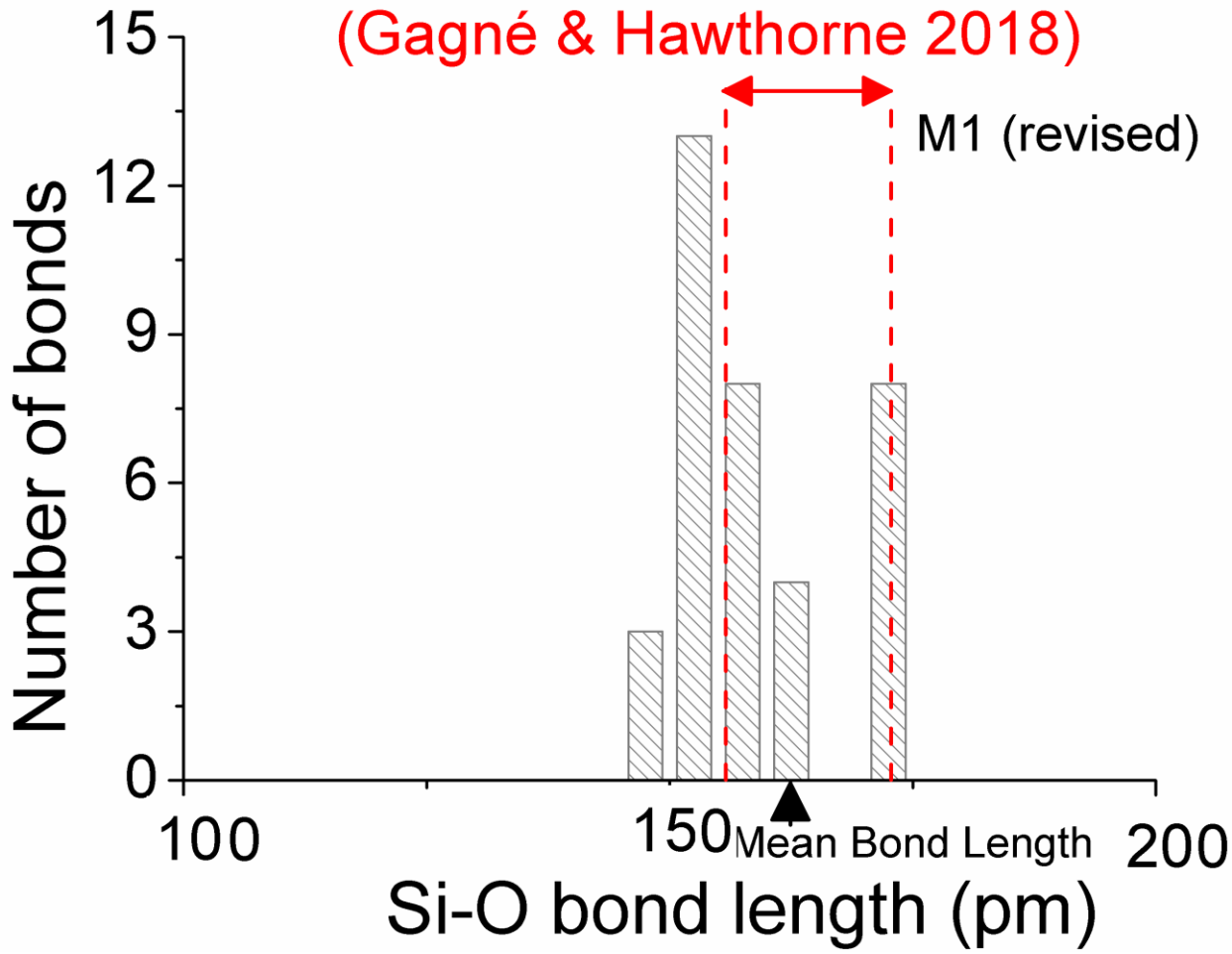

Figure 6 Histogram of BVS error of Ca valence according to Noirfontaine's a) and proposed M1 polymorph structural model (b).

a)

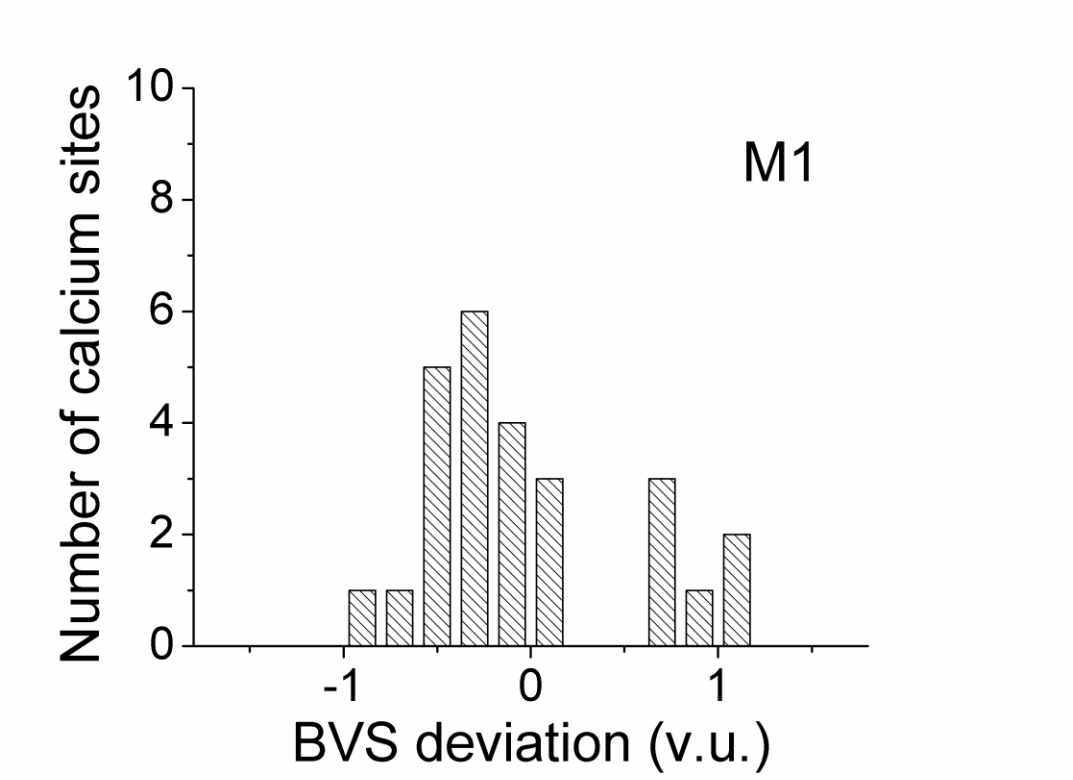

b)

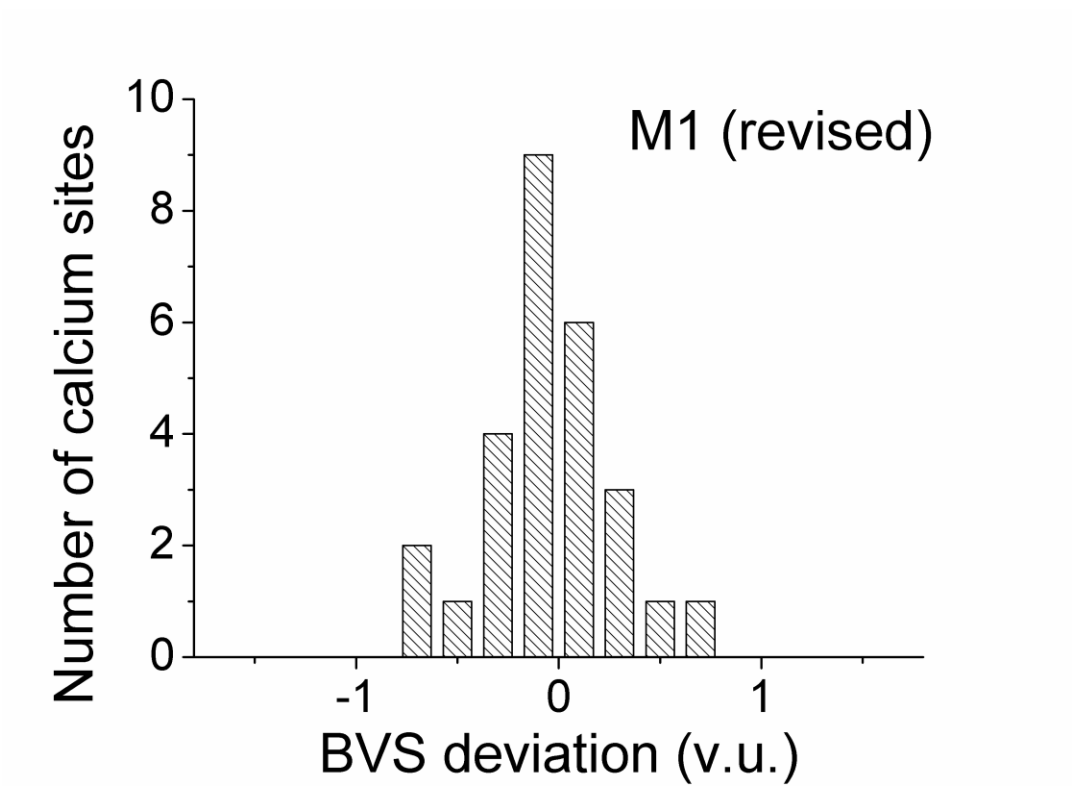

Figure 7 Histogram of BVS error of Si valence according to revised M1 polymorph structural model.

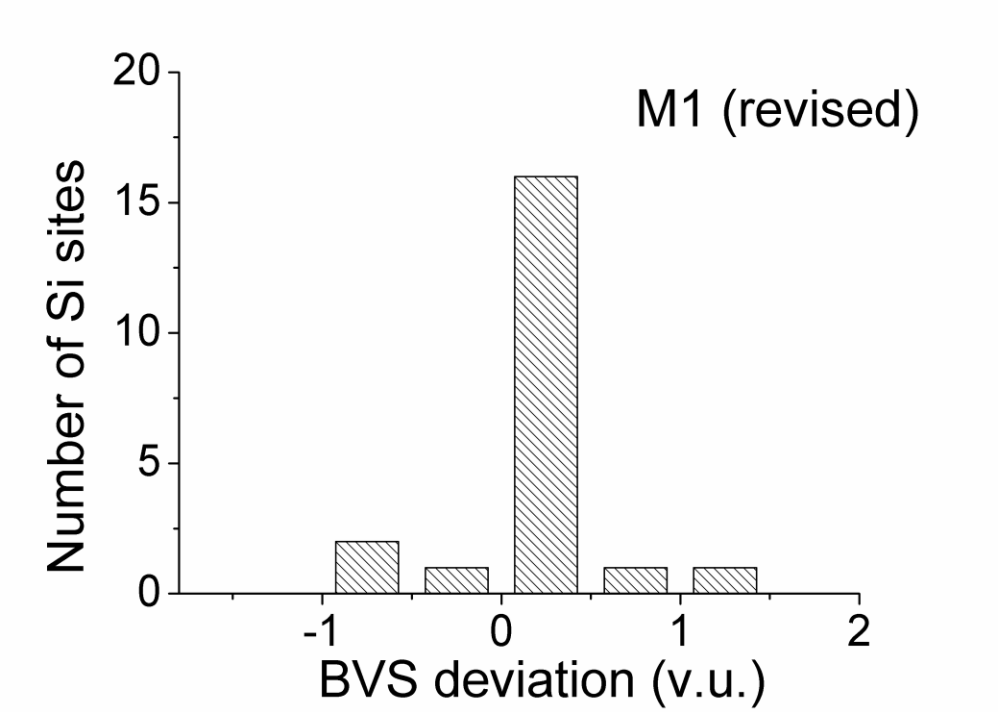

Figure 8 Possible preferential sites against the occupancy percentage of minor constituent calculated by BVS method.

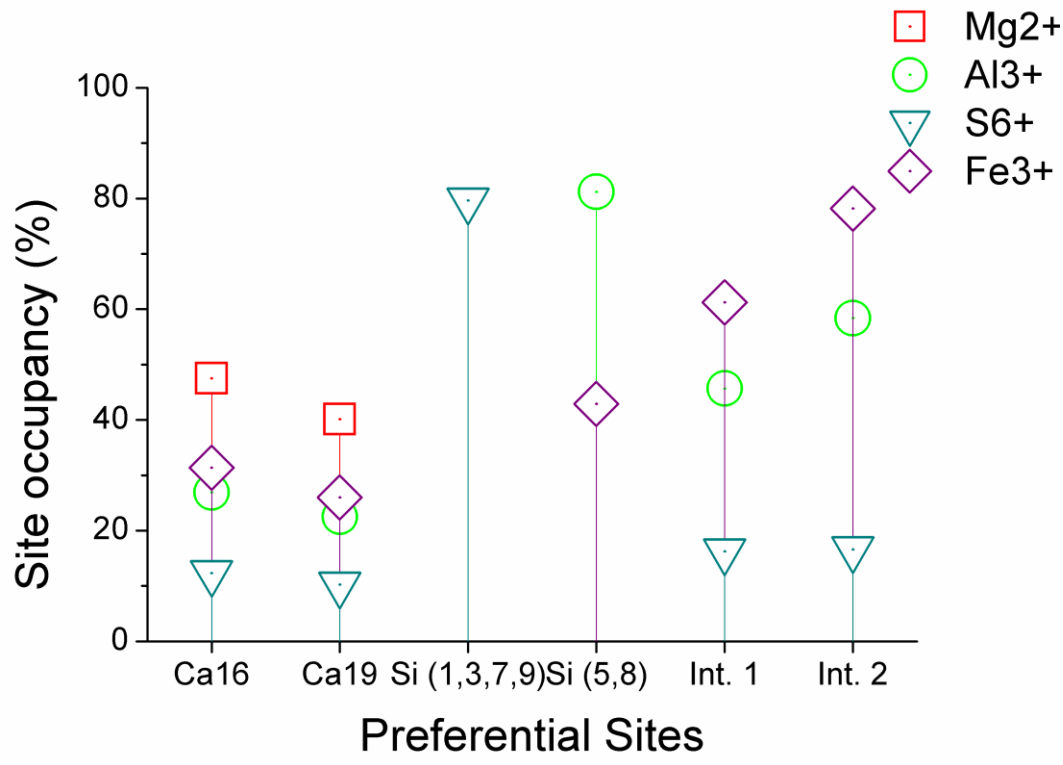

Figure 9 Plot of Cation:Ca ratio as a function of Si:Ca ratio from EPMA of the industrial clinker sample and BVS calculations.

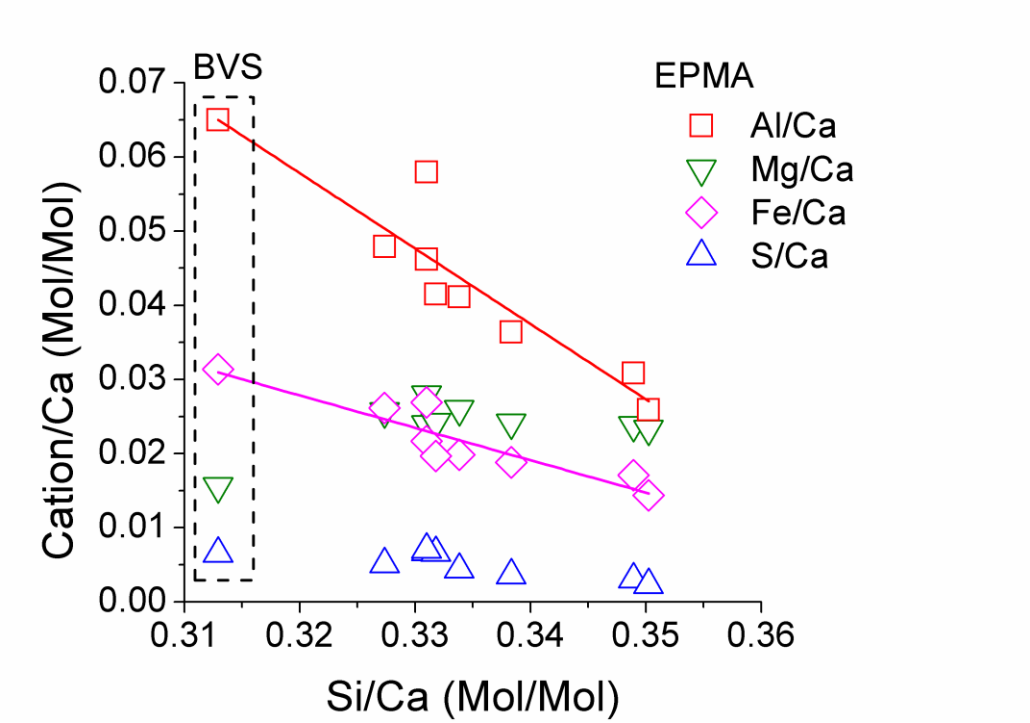

Figure 10 Comparison of the observed (blue dot), calculated (red) and difference (grey) profiles from Rietveld refinement of synchrotron PXRD data range (from 17 to 18.3 2θ°) of six industrial clinker samples using revised C3S M1 model and the Noirfontaine M1 Model, showing calculated phases profiles of alite M1 (light blue), alite M3 (black), belite (light green), aluminate (dark green) and ferrite (purple).

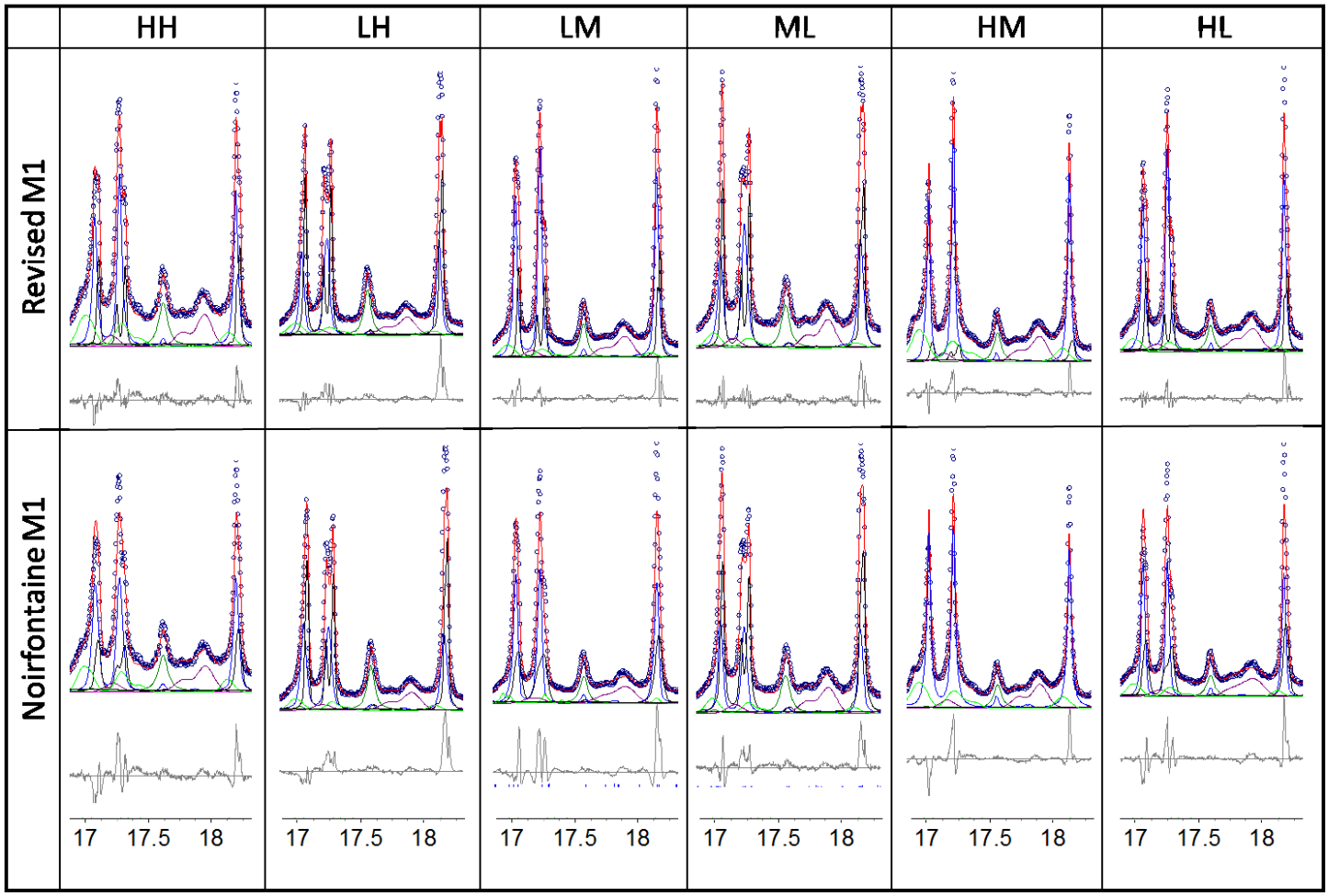

Figure 11 Comparison of Rietveld QPA result of 6 industrial clinker samples using revised C3S M1 model (a) and Noirfontaine's M1 Model (b).

a)

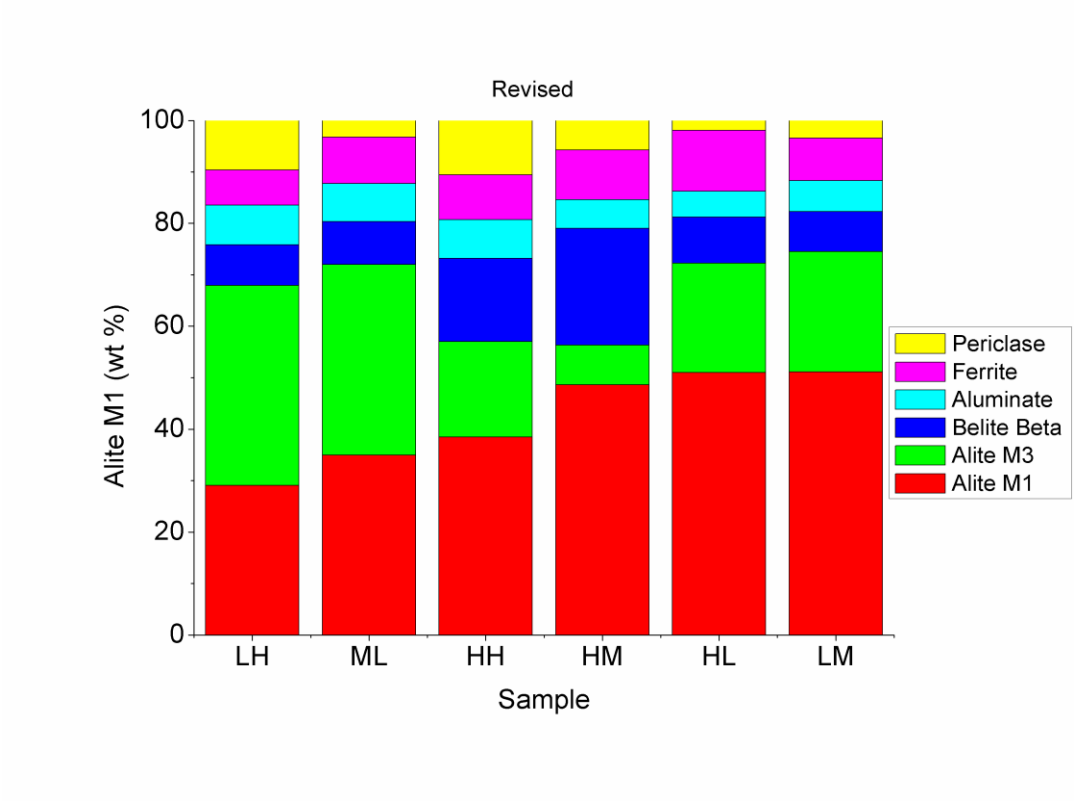

b)

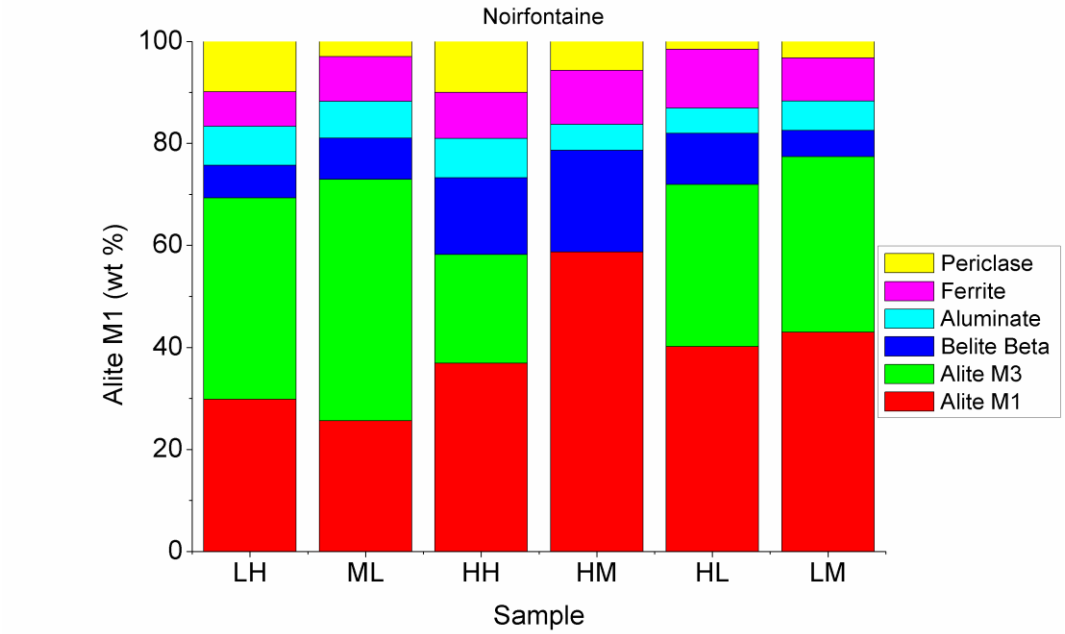

Figure 12 Comparison of the amount of alite Polymorph (a) and the amount of other phases (b) obtained through Rietveld QPA of 6 industrial clinker samples using revised C3S M1 model and Noirfontaine's M1 Model.

a)

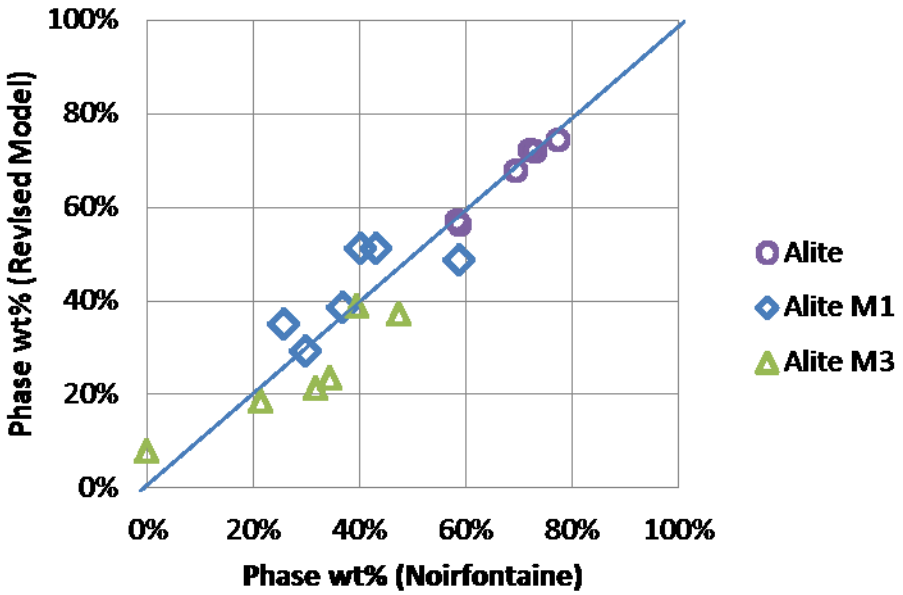

b)